PARAMETRIC EFFECT OF THE INTERRUPTED ANNULAR GROOVE FIN ON FLOW AND HEAT TRANSFER CHARACTERISTICS OF A FINNED CIRCULAR TUBE HEAT EXCHANGER

by

Zhimin LIN**, Ruixia YANG, Haihong YANG, Liangbi WANG, Yongheng ZHANG, and Anning GUO

School of Mechanical Engineering,
Key Laboratory of Railway Vehicle Thermal Engineering of MOE,
Lanzhou Jiaotong University, Lanzhou, Gansu, China

Original scientific paper
https://doi.org/10.2298/TSCI211015040L

The influences of the geometrical parameters of interrupted annular groove fin mainly including the annular groove diameter, the groove arc length, and the fin spacing, on the fin side thermal-hydraulic characteristics of a finned circular tube exchanger were numerically investigated by actualizing the custom FORTRAN programing with SIMPLE algorithm in a non-orthogonal curvilinear co-ordinate system, and the regression formulas of average Nusselt number and friction factor with flow parameters and geometrical parameters were obtained. Compared with the referential plain fin, interrupted annular groove fin could significantly improve thermal performance under the same pumping power constraint, and Nusselt number is closely germane to the secondary flow, which implies that the fin side heat transfer is depended entirely on the secondary flow strength. For Nusselt number, the annular groove diameter and the groove arc length have positive effect, while the fin pitch, the groove circumferential and radial locations have negative effect. The dominant parameters influencing on friction factor in turn are the fin pitch, the groove radial location, and the annular groove diameter. The optimal annular groove diameter is screened, and found that the optimal annular groove diameter is closely related with Reynolds number under the same pumping power constraint, while under the same mass-flow rate constraint that is scarcely related with Reynolds number.

Key words: *finned tube heat exchanger, heat transfer augmentation, interrupted annular groove fin, numerical simulation*

Introduction

Finned circular tube heat exchangers are extensively applied in multifarious industrial fields, the fins not only work as extended surfaces, but also can influence the flow structure and furthermore influence heat transfer ability especially for fins having 3-D features. The thermal performance of this type of heat exchanger is dominated primarily by the fin's heat transfer ability due to the majority of thermal resistance being on the fin side. A practical method to solve such problem is to develop the enhanced fin patterns through variations in fin surface geometry [1-6]. The physical reasoning of the innovative fin designs for enhancing heat transfer has been clearly disclosed, mainly including increasing the heat transfer area, extending the streamwise

* Corresponding author, e-mail: linzhimin@mail.lzjtu.cn

distance, restarting the thermal boundary-layer by means of repeated geometries, or producing flow disturbance and swirl flow.

When the air-flows across finned circular tube, the streamline becomes critically deteriorated and a separation wake zone would unavoidably appear behind the circular tube, which results in a remarkable increasing of the friction loss in the zone near the front and rear stagnation points of circular tube, and a declining of the fin heat transfer ability in the tube re-circulation zone. Experts know that the wavy fin, the louvered fin, and the slotted fin are less efficient to diminish the size of the re-circulation zone. Many studies have shown that if appropriate vortex generator (VG) are introduced, the size of re-circulation zone would be efficiently decreased, which is closely related to the geometry and location parameters of VG, Reynolds number, and different tube arrangements [7-17]. Torii *et al.* [7] and Allison and Dally [8] found the re-circulation area that worsens heat transfer could be effectively removed by using plane VG positioned in the common flow up (CFU) manner. He *et al.* [9] informed that longitudinal vortices induced by plane VG in CFU manner could strengthen the mixing of the hot and cold fluids and diminish the size of the re-circulation zone. Naik and Tiwari [10] revealed that the position of VG plays an important role in affecting the fin side thermal properties in presence of plane rectangular VGs punched upstream tube. Huisseune *et al.* [11] proposed a compound design of the louvered fins with plane delta-winglet VG, and revealed that this kind of combinatorial fin could thin the boundary-layer, better flow mixing and delay flow separation, which lead to a remarkable heat transfer augmentation. Variation in VG geometry is an alternative strategy to ameliorate the fin side thermal performance. Leu *et al.* [12] demonstrated the inclined block shape VG could not only produced the secondary flow but also defer boundary-layer separation reduce the size of the re-circulation zone, and these effects are more pronounced as the Reynolds number increases. A novel fin punched with body fitted curve winglet VG at the rear of circular tube is proposed by Gong *et al.* [13] and Lin *et al.* [14-16] for finned circular tube exchanger. The numerical calculation indicated that those curve winglet VG positioned behind each circular tube could not only generate secondary flow but also aid the air pass into the tube re-circulation zone. Oh and Kim [17] numerically investigated the influences of position of three different winglet curve VG (rectangular winglet, delta-winglet upstream, and delta-winglet downstream) on the thermal-hydraulic characteristics of a finned circular tube heat exchanger. In real applications, however, VG are generally punched from and on the fin surface. Consequently the holes left in the punching process will cut the conduction paths in the fin along the circular tube radial direction which is an unfavorable factor for fin side heat transfer augmentation.

In comparison with the fin patterns mentioned previously, the interrupted annular groove fin (IAGF) is suitable for finned circular tube exchanger. It has four annular groove structures around each tube, as shown in fig. 1. The upstream grooves can be viewed as the flow redistributors to guide fluid for better streamline pattern, while the downstream ones can delay flow separation decrease the size of re-circulation zone. Moreover, the secondary flow would be produced by the interrupted annular grooves (IAG) when the fluid-flows over the grooves, on the other hand, the discontinue annular grooves are formed by partly cutting and then punching on the basic of the fin surface, which is similar to the molding process of the slotted fins. The heat transfer area is extended and the thermal boundary-layer would be periodically redeveloped by the annular grooves. Moreover, the punched annular grooves do not obstruct the conduction paths of the fins along the radial direction. Thus, IAGF can be taken as a combination of kinds of heat transfer augmentation mechanisms. However, owing to the complexity of the IAGF structure, the physical reasoning of heat transfer augmentation for this fin pattern is less studied. Wang *et al.* [18] conducted the flow visualization of the channel region constituted by the circular tube bank annular groove fins, and they found longitudinal vortex pairs appear back the circular tube, and the longitudinal vortices strength increases when the height of annular grooves is heightened, but the heat transfer behavior was not discussed in their study. Lin *et al.* [19] conducted the thermal and flow characteristics in the fin side of a heat exchanger incorporated with staggered circular tube bank fins punching IAG into the fin surfaces.

Moreover, to guide the optimization design of the finned circular tube exchanger with IAGF, it is imperative to discuss the geometric influences of IAGF on the thermal performance. Some literature has reported on exploring the comprehensive performance of the circular finned tube exchanger by using IAGF. Jiang [20] experimentally investigated the influence of the fin pitch on the thermal and turbulent flow characteristics of IAGF by using the naphthalene sublimation analogy method. In contrast to the referential plain fin (PF), the results showed that with higher Reynols number the thermal performance of IAGF is obviously strengthened when the fin pitch heightens, while the heightened the fin pitch has little influence on the friction loss. Zhang *et al.* [21] discussed the airside performance of IAGF at high Reynols number condition of turbulent flow by numerical method, in which the studied geometrical parameters mainly including the tube row numbers, the fin spacing and the attack angles of the annular groove. Their results indicated that the tube row numbers, the fin pitch, and the attack angle of the annular groove have their critical values for heat transfer augmentation. But the geometry parameters of IAG themselves are rarely involved. Lin *et al.* [19] numerically studied the parametric influence of the annular groove circumferential and radial locations on the fin side thermal performance. They found that the radial position of the annular grooves obviously affects the thermal performance of laminar flow at the studied high Reynolds numbers. The circumferential position almost had no effect on heat transport and the friction factor, but increasing the angle between the annular groove and the tube center line can guide the fluid pass though the tube with less pressure drop. However, because the main propose of their study is to inquire into the physical mechanism for heat transfer augmentation of IAGF, therefore, only limited fin parameters are addressed in their study. So far there is no available information about the parametric effects of IAGF on the fin side thermal performance. In view of this fact, the present paper is aimed to ascertain the parameter influences of IAGF on thermal-hydraulic characteristics for further optimizing design of such fin. Furthermore, to facilitate easy application, the data obtained by the present study and the published data [19] are included in the same regression formulas of Nusselt number and the friction loss coefficient of IAGF.

Physical model

Figure 1 presents the studied heat exchanger, which is formed by two circular tube rows and several IAGF. The characteristic of this fin pattern is that the half annular grooves symmetrically distribute around the tube both along the longitudinal and the transversal directions. These IAG are punched from and on the fin surfaces.

The geometrical parameters of IAGF mainly include: the number of the longitudinal rube row, N, the longitudinal tube distance, S_2, the horizontal tube distance, S_1, the fin length, L_f, the tube outer diameter, D, the fin spacing, T_p, the inner and outer circular diameters, D_1 and D_2, to indicate the radial location of the annular groove and its size, and the latter can also use the diameter of the annular groove $D_g = (D_2 - D_1)/2$ to mark, θ used to describe the circumferential length of annular groove, and β to identify the circumferential position of annular groove. The definition of the geometrical parameters is shown in fig. 2. The central parameter values are: $N = 2$, $S_1 = 26.0$ mm， $S_2 = 21.0$ mm， $D = 9.0$ mm, $T_p = 2.2$ mm, $D_1 = 12.0$ mm, $\theta = 40°$, 50°, and 60°, $\beta = 25°$, 20°, and 15°. In this study, D_1 is constant and D_2 varies to get different D_g of 2.0 mm, 2.5 mm, 3.0 mm, 3.5 mm, and 4.0 mm.

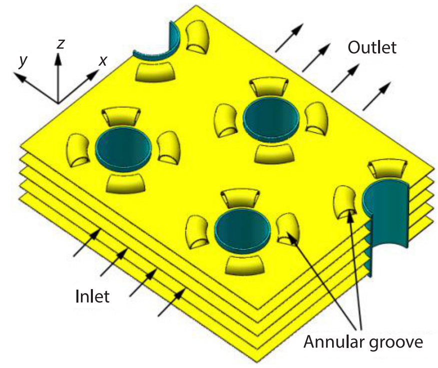

Figure 1. The studied finned tube exchanger with IAGF

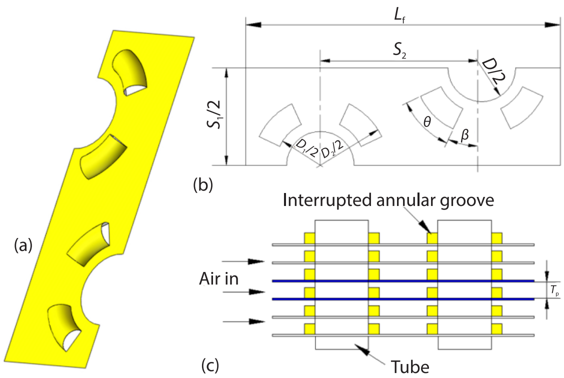

Figure 2. Fin geometry; (a) fin with IAG, (b) vertical view and its main parameters, and (c) front view

The simulation region is the air-flow channel formed by two rows tube and two neighbor IAGF as shown in fig. 3. To save computational time, the non-conjugated heat transfer model is used. Thus, the top and bottom boundaries of the computational model are the two neighbor fin surfaces with zero thickness. To ensure the accuracy of the commonly used boundary condition named as local-unidirectional assuming which is enforced at the outlet, the re-circulation flow is necessarily avoided. Thus, the simulation region is lengthened with two times tube diameter after the physical exit.

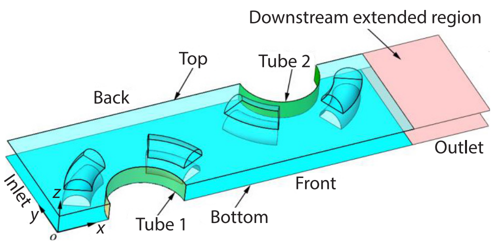

Figure 3. Simulation region and its boundaries

Theoretical formulation

Governing equations

The assumed conditions are made to develop numerical model:
– the physical properties of the working medium are constant,
– the fluid is considered as incompressible and the flow is in a steady laminar state,
– in energy equation the viscous dissipation term is not considered, and
– the temperatures on the tube wall and fin surface are uniform.

The governing equations are given as following.

Mass conservation equation:

$$\frac{\partial}{\partial x_i}(\rho u_i) = 0 \tag{1}$$

Momentum conservation equation:

$$\frac{\partial}{\partial x_i}(\rho u_i u_j) = -\frac{\partial p}{\partial x_j} + \mu \frac{\partial}{\partial x_i}\left(\frac{\partial u_j}{\partial x_i}\right), \quad (j = 1, 2, 3) \tag{2}$$

Energy conservation equation:

$$\frac{\partial}{\partial x_i}(\rho c_p u_i T) = \frac{\partial}{\partial x_i}\left(\lambda \frac{\partial T}{\partial x_i}\right) \tag{3}$$

Boundary conditions

At the inlet, the uniform inflow velocity and uniform temperature are enforced:

$$u(x,y,z)=u_{\text{in}},\ v(x,y,z)=w(x,y,z)=0,\ T(x,y,z)=T_{\text{in}} \tag{4}$$

At the outlet, the local-unidirectional assuming [22] is used for either velocity or temperature:

$$\frac{\partial u(x,y,z)}{\partial x}=\frac{\partial v(x,y,z)}{\partial x}=\frac{\partial w(x,y,z)}{\partial x}=\frac{\partial T(x,y,z)}{\partial x}=0 \tag{5}$$

The symmetry boundary condition is enforced for flow region at the front and back sides:

$$\frac{\partial u(x,y,z)}{\partial y}=\frac{\partial w(x,y,z)}{\partial y}=\frac{\partial T(x,y,z)}{\partial y}=0,\ v(x,y,z)=0 \tag{6}$$

while for tube wall at the front and back sides:

$$u(x,y,z)=v(x,y,z)=w(x,y,z)=0,\ T(x,y,z)=T_{\text{w}} \tag{7}$$

At the top and bottom boundaries, the symmetry boundary condition is used for the downstream extension area:

$$\frac{\partial u(x,y,z)}{\partial z}=\frac{\partial v(x,y,z)}{\partial z}=\frac{\partial T(x,y,z)}{\partial z}=0,\ w(x,y,z)=0 \tag{8}$$

and for fin region, the non-slipping condition for velocity and uniform temperature are used:

$$u(x,y,z)=0,\ v(x,y,z)=0,\ w(x,y,z)=0,\ T(x,y,z)=T_{\text{w}} \tag{9}$$

while periodic boundary condition is enforced for the inlet and the outlet of the annular groove region:

$$u(x,y,0)=u(x,y,T_{\text{p}}),\ v(x,y,0)=v(x,y,T_{\text{p}}),\ w(x,y,0)=w(x,y,T_{\text{p}}),\ T(x,y,0)=T(x,y,T_{\text{p}}) \tag{10}$$

Definition of relative parameters

Reynolds number and average Dancy friction factor is, respectively defined:

$$\text{Re}=\frac{\rho u_{\text{in}}D}{\mu},\ f=\frac{2\Delta pD}{\rho u_{\text{in}}^2 L_{\text{f}}} \tag{11}$$

where D is the tube outside diameter, L_{f} – the fin length, and Δp – the pressure drop from the inlet to the physical outlet cross-sections.

The local heat transfer coefficient is defined:

$$h_{\text{local}}=-\frac{\lambda\left(\dfrac{\partial T}{\partial n}\right)}{(T_{\text{w}}-T_{\text{f}})} \tag{12}$$

where the reference temperature $T_{\text{f}} = (T_{\text{in}} + T_{\text{out}})/2$ proposed by [23], T_{in} and T_{out} are respectively the cross-section bulk temperature at the inlet and outlet.

The local and average Nusselt numbers are defined:

$$\text{Nu}_{\text{local}}=\frac{h_{\text{local}}D}{\lambda},\ \text{Nu}_{\text{m}}=\frac{\iint_s \text{Nu}_{\text{local}}\text{d}s}{\iint_s \text{d}s} \tag{13}$$

The definition of the secondary flow strength and how to use it have been discussed in detail in [24-26]. The volumetric average absolute vorticity flux is introduced:

$$J_{\mathrm{ABS}}^{n} = \frac{1}{V}\iiint_{V} |\omega^{n}|\,\mathrm{d}V \tag{14}$$

Accordingly the volumetric average dimensionless parameter is introduced to describe the secondary flow strength [26]:

$$Se_{\mathrm{m}} = \frac{\rho J_{\mathrm{ABS}}^{n} D^{2}}{\mu} = \frac{\rho D^{2}}{\mu}\frac{\iiint_{V} |\omega^{n}|\,\mathrm{d}V}{\iiint_{V}\mathrm{d}V} \tag{15}$$

Numerical method and its validation

Grid generation and numerical method

The combination of the double boundary method [27] and the infinite interpolation method [28] to generated the preliminary mesh, and then by solving the Poisson equation improve the local mesh distribution. A typical grid system is shown in fig. 4. There are mainly five local regions including the circular tube region, the fin surface region, annular grooves region, fin channel region and the extended fluid region. To capture the accurate geometrical parameters of the fin, the grid distribution in *x-y-z* co-ordinates should be modified repeatedly. After carefully modifying, a suitable grid system is shown in figs. 4(a)-4(c).

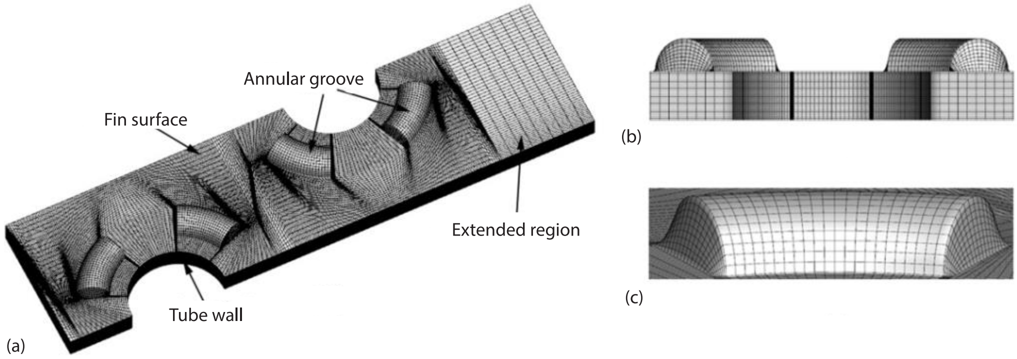

Figure 4. The grid system for the simulation region; (a) global grid, (b) local grid of the tube, and (c) local grid of the annular groove

The governing equations shown in eqs. (1)-(3) are transformed into the ones in the body-fitted co-ordinate. Then the governing equations are integrated over a cell volume to obtain the corresponding algebraic equations by using control volume method. The SGSD scheme proposed in [29] is employed for the convection terms, while the central difference scheme is imposed for the diffusion terms. In the flow regions, the SIMPLE algorithm was used to deal with the coupling of velocity and pressure [22], to overcome the decoupling between them, the concept of momentum interpolation of [30] is applied. Aforementioned numerical methods are written in the code by our group.

Grid independency validation

The assessment of the grid-independence of the numerical simulation is compulsory. During the assessment process, three grid systems of 270 × 39 × 25, 302 × 49 × 30, and

342 × 59 × 35 are used and evaluated for the physical model with geometry size of S_1 = 26.0 mm, S_2 = 21.0 mm, D = 9.0 mm, T_p = 2.2 mm, D_1 = 12.0 mm, D_g = 3 mm, θ = 40°, and β = 25°. The numerical results of $\mathrm{Nu_m}$ and f with different mesh numbers are seen in tab. 1. By comparing the values of $\mathrm{Nu_m}$ and f, one cannote that the relative variations of $\mathrm{Nu_m}$ is less than 2.5%, and the relative variations of f is less than 1.5%, which could be considered the grid independence is appropriate. In this study, the grid system of 302 × 49 × 30 is used in the simulation. For various fin geometry models, the grid size would be slightly adjusted.

Table 1. Results of the different grids tested

Grid numbers	Re	$\mathrm{Nu_m}$	f
270 × 39 × 25	1010	18.921	1.6728
302 × 49 × 30	1010	19.116	1.6877
342 × 59 × 35	1010	19.393	1.6927
Maximum error	–	2.43%	1.18%

Validation of the numerical method

The thermal and flow characteristics in the fin side of exchanger incorporated with four rows circular tube and IAGF were numerically investigated by Lin *et al.* [19]. To validate the appropriateness and accuracy of computational method, the same physical model as used by Lin *et al.* [19] is selected, and under the same Reynolds number condition, $\mathrm{Nu_m}$ and f are compared. The comparison of $\mathrm{Nu_m}$ and f indicates that the present calculated data agree well with the available numerical ones, the maximum differences of $\mathrm{Nu_m}$ and f are, respectively 12.1% and 5.8%. The reason for selecting the numerical results to validate the computational method used in present study is that for one aspect there is less available experimental data on IAGF element, and for other aspect the numerical method used in Lin *et al.* [19] is quite different from that used in this study. We consider that when two different numerical methods are used for the same model, if approximate results could be obtained within the scope of acceptance, it is believed that the used numerical method is reasonable and credible.

The results and discussion

Influences of the annular groove diameter

Five different D_g is used to explain the influences of the annular groove diameter on the thermal and flow characteristics. Under the identical other parameters condition, $\mathrm{Nu_{local}}$ on the bottom and the top surfaces for PF and IAGF with five different D_g are, respectively shown in figs. 5(a) and 5(b). It is found that $\mathrm{Nu_{local}}$ is large in the region close to the inlet. For IAGF, $\mathrm{Nu_{local}}$ is large in the region and nearby area where the grooves located due to the existence of grooves. This declares that the IAG have obvious role in heat transfer augmentation. The reason is that as the air-flows through the area where the grooves located, the flow and thermal boundary-layers are interrupted and redeveloped. In addition, with increasing the groove diameter D_g, the re-circulation zones occurred in the rear part of the circular tubes decreases, thus the heat transport capacity increases in this area. From the other view point the existence of the IAG would extra induce the secondary flow, which could also enhance heat transfer. The decrease of the re-circulation zones and the increase of the secondary flow strength to enhance heat transport would be discussed in the following sections.

The reported results by Lin *et al.* [19] revealed that IAGF has a good efficacy of delaying flow separation decrease the size of tube re-circulation area. To find the effect of different groove diameter on this eddy inhibition, figs. 6(a)-6(d) illustrate the 3-D streamline of PF and IAGF with three different D_g when T_p = 2.2 mm and Reynolds number changes from 600-2500, respectively. As show in fig. 6, compared with that of PF, in virtue of the appearance of IAG the streamline is interrupted as fluid-flows through them, and then under the guide of the annular grooves the fluid-flows downstream, which results in the wake zone being significantly inhibited. Moreover, the discontinue annular grooves also results in the flow boundary-layer being interrupted, thus, the flow becomes more complex. By comparing the results shown in figs. 6(a)-6(d), one cannote that the size of tube wake zone decreases when the groove diameter D_g increases, further the heat transfer ability would be enhanced. However, the flow field becomes more complex which would lead to increase in pressure drop penalty. Therefore, for a given fin spacing, the groove diameter should be screened to obtain better heat transport performance but with small increase in pressure drop penalty.

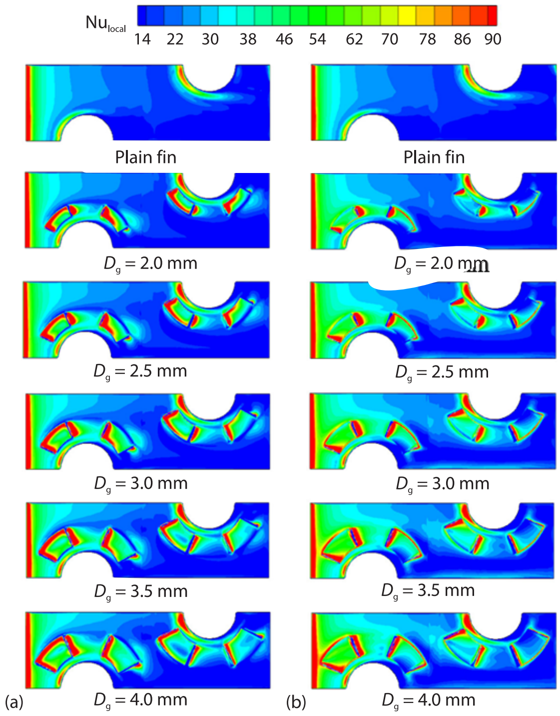

Figure 5. Distribution of Nu$_{local}$ of PF and IAGF with five different D_g; (a) Nu$_{local}$ on the bottom surface and (b) Nu$_{local}$ on the top surface

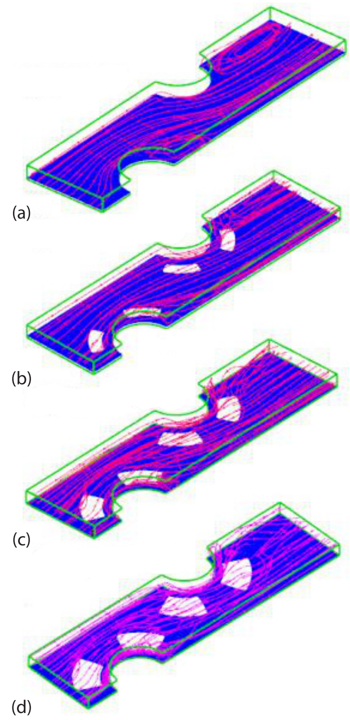

Figure 6. The 3-D streamlines in the channel; (a) PF and (b)-(d) IAGF with three different D_g = 2.0, 3.0, and 4.0 mm, respectively

Figures 7(a) and 7(b) present the effects of the groove diameter D_g on Nu$_m$, and f when Reynolds number changes from 600-2500, respectively. As seen in fig. 7(a), under the same D_g condition, Nu$_m$ enhances with increasing Reynolds number, and as Reynolds number is the same, Nu$_m$ enhances with increasing D_g. But for the lower Reynolds number, Nu$_m$ increases slightly with increasing D_g, while for the higher Reynolds number, Nu$_m$ enhances obviously with increasing D_g. As seen from fig. 7(b), under the same D_g condition, f decreases when Reynolds number increases, and under the same Reynolds number condition, f also increases as D_g increases. The reason is that under the same T_p and Reynolds number conditions, the flow area of the channel would be decreased when D_g increases. This implies that for different T_p and Reynolds number, D_g should be carefully selected to obtain the optimal heat transfer performance.

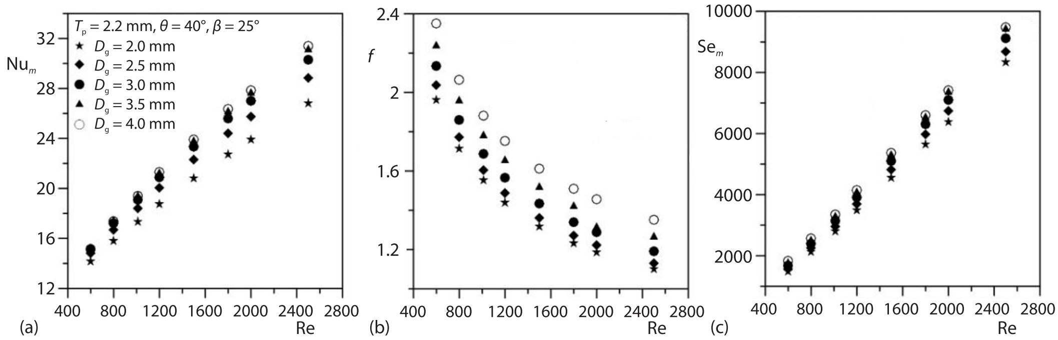

Figure 7. Effects of D_g on Nu_m, f, and Se_m as a function of Reynolds number changing from 600-2500 when θ = 40°, T_p = 2.2 mm, and β = 25°; (a) Nu_m, (b) f, and (c) Se_m

As previously mentioned, the secondary flow is an advantageous factor to strengthen heat transfer. To ascertain the change of the secondary flow strength caused by different D_g and to deep interpret the role of secondary flow to heat transfer augmentation, fig. 7(c) presents the effect of D_g on Se_m as a function of Reynolds number varied from 600-2500. As seen in fig. 7(c), for PF and IAGF cases, when Reynolds number increases, the secondary flow strength also increases, and the secondary flow strength of IAGF is obviously larger than that of PF at a given Reynolds number, especially for the cases of higher Reynolds number. This is because when the flow velocity increases, the gradients of velocity components inside the channel also unavoidably increase, and these velocity components with too large gradient would produce large flow resistance along the mainstream direction. Thus, the velocity components and their gradients on the transversal surface normal to the mainstream direction increase to strengthen the secondary flow strength. The aforementioned trend would bring about an increase in Nu_m and f, as shown, respectively in figs. 7(a) and 7(b).

Influence of the groove arc length

The groove arc length is indicated by θ, see fig. 2. When the other parameters are the same, *i.e.* D_g = 3.0 mm and T_p = 2.2 mm, figs. 8(a)-8(c) illustrates the effects of groove arc length with three different value of θ = 40º, 50º, and 60º on Nu_m, f, and Se_m when Reynolds num-

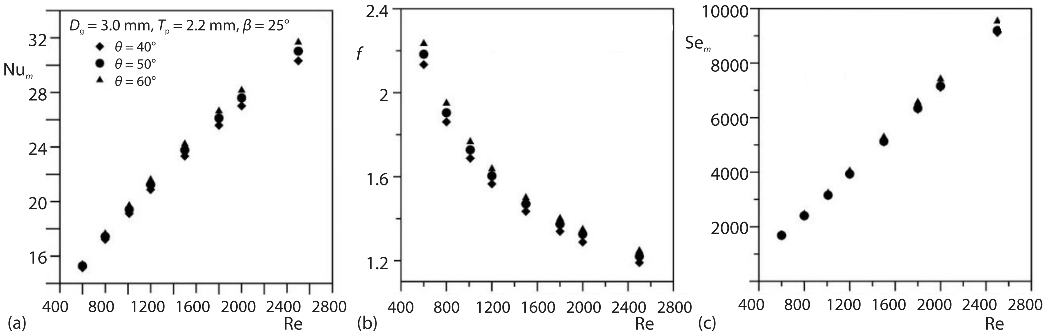

Figure 8. Effects of groove arc length indicated by θ on Nu_m, f, and Se_m as a function of Reynolds number changing from 600-2500 when D_g = 3.0 mm, T_p = 2.2 mm, and β = 25°; (a) Nu_m, (b) f, and (c) Se_m

ber changes from 600-2500, respectively. As seen in figs. 8(a) and 8(b), either Nu_m or f increases slightly as θ increases for studied Reynolds number, and the increase of Nu_m is relatively weaker for the lower Reynolds number, which illustrates under the same other conditions increasing the large arc length is not a favorable factor to improve heat transport performance. To explain how the variation of the arc length of the annular groove affect the secondary flow strength, fig. 8(c) presents the relationship between Reynolds number and Se_m for different groove arc length of θ = 40º, 50º, and 60º when Reynolds number ranges from 600-2500. For IAGF case, the secondary flow strength is weakly dependent on the arc length θ, as seen in fig. 8(c).

Influence of the fin spacing

When the other parameters are given, *i.e.* D_g = 2.0 mm and θ = 40°, fig. 9 illustrates the effects of fin spacing with four different T_p on Nu_m, f, and Se_m when Reynolds number changes from 600-2500. As seen in figs. 9(a) and 9(b), either Nu_m or f obviously decreases as T_p increases, especially for the cases of lower Reynolds number. This may be ascribed to the stronger disturbance of fluid for small T_p. Thus, the comprehensive heat transport performance are closely dependent on the fin spacing, which may provide a clue to obtain the optimal heat transfer performance by screen appropriate fin spacing. As seen in fig. 9(c), when the other parameters are identical, the fluid disturbance becomes weaker as T_p increases. Thus, the secondary flow strength decreases with increasing T_p, and the downtrend of the secondary flow strength is more obvious with increasing Reynolds number. These results illustrate that IAGF may generate more intense secondary flow for the case with small T_p and then strengthen convective heat transfer effectively.

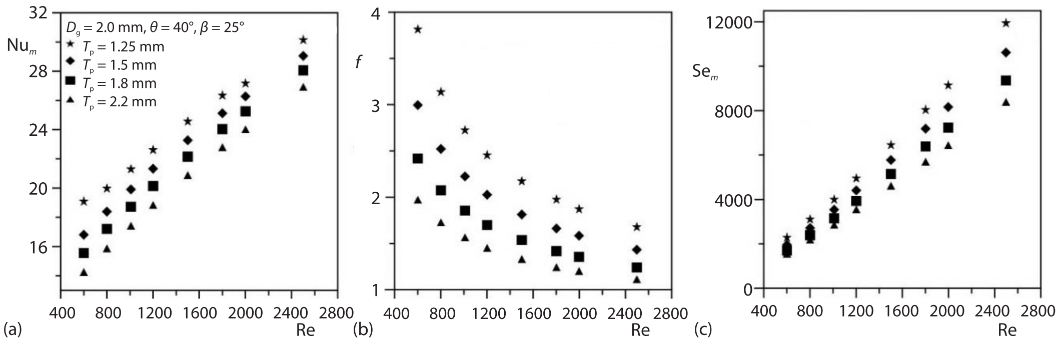

Figure 9. Effects of T_p on Nu_m, f, and Se_m as a function of Reynolds number changing from 600-2500 when D_g = 3.0 mm, θ = 40° and β = 25°; (a) Nu_m, (b) f, and (c) Se_m

Evaluation of heat transfer augmentation

Thermal performance factors JF_1 and JF_2 are used to appraise the thermal performance of IAGF under the same pumping power and the same mass-flow rate constraints, respectively. These criteria are [31]:

$$JF_1 = \frac{\left(\dfrac{\mathrm{Nu_m}}{\mathrm{Nu_{m,plain}}}\right)}{\left(\dfrac{f}{f_{\mathrm{p,lain}}}\right)^{1/3}}, \ \left(\text{under identical pumping power constraint}\right) \tag{16}$$

$$JF_2 = \frac{\dfrac{\mathrm{Nu_m}}{\mathrm{Nu_{m,plain}}}}{\dfrac{f}{f_{\mathrm{plain}}}}, \ \left(\text{under identical mass-flow rate constraint}\right) \tag{17}$$

Figures 10(a) and 10(b) present the value of JF_1 and JF_2 with identical T_p = 2.2 mm, θ = 40°, and β = 25° but with five different D_g and different Reynolds number changing from 600-2500. As seen in fig. 10(a), almost all JF_1 are larger than 1.0 for studied cases. This indicates that the thermal performance of IAGF is prior to that of PF under the same pumping power constraint. When the other parameters are the same, JF_1 increase with increasing Reynolds number except for the case of D_g = 2 mm. For the cases with different D_g and the same other parameters, one cannote that JF_1 increases with increasing D_g firstly, and then begins to decline after reaching the maximum value, which indicates that under the same pumping power constraint, there is an optimal D_g to obtain the best heat transfer performance as only D_g changes, and the optimal value of D_g is also dependent on Reynolds number. For studied cases of higher Reynolds number changing from 1500-2500, the optimal D_g is about 3.5 mm, while for studied cases of lower Reynolds number changing from 600-1500, the optimal D_g is about 3.0 mm. This indicates that in the practical application the flow condition should be considered to select the appropriate D_g. However, JF_2 are less than 1.0 for studied cases, as seen in fig. 10(b). This indicates that under the same mass-flow rate constraint, using IAGF could not effectively improve thermal performance of finned tube exchanger. Meanwhile, as the other parameters are given, JF_2 increase with the increasing of Reynolds number when Reynolds number is larger than 1010, while JF_2 is scarcely dependent on Reynolds numbe for studied cases of lower Reynolds number ranging from 600-800. For the cases with different D_g and the same other parameters, one can also note that with increasing D_g, JF_2 increases firstly and then declines when D_g is larger than 2.5 mm. This means the optimal D_g = 2.5 mm which could obtain the best heat transfer performance under the same mass-flow rate constraint, and the optimal value of D_g is scarcely dependent on Reynolds number for studied cases.

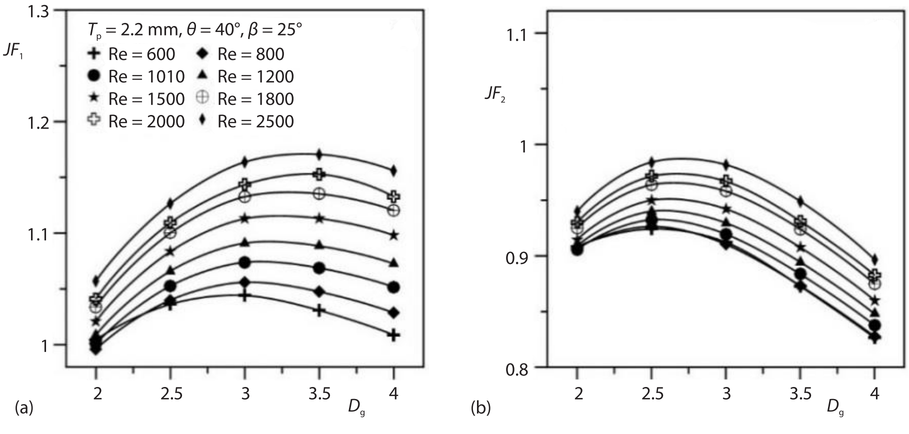

Figure 10. The relationship between thermal performance factor *JF* and groove diameter D_g at different Reynolds number; (a) JF_1 and (b) JF_2

Figs. 11(a) and 11(b), respectively presents the value of JF_1 and JF_2 with identical T_p = 2.2 mm, D_g = 3.0 mm, and β = 25° but with different arc length of the annular groove designated by θ (θ = 40°, 50°, and 60°) and different Reynolds number ranging from 600 to 2500. As shown in fig. 11(a), under the same other parameters, the variation tendency of JF_1 with the increasing θ is dependent on Reynolds number. For studied cases of lower Reynolds number such as Re = 600, JF_1 is almost constant as θ increases, while for studied cases of higher Reynolds number ranging from 800 to 2500, JF_1 increases as θ increases, and the growth rate increases with increasing Reynolds number. This means that increasing the arc length of annular groove is not a favorable measure to improve thermal performance. As seen in fig. 11(b), under the same other parameters, the variation tendency of JF_2 with the increasing θ is also dependent on Reynolds number. Compared with that of JF_1, the difference is that for the cases of lower Reynolds number ranging from 600-1200, JF_2 decreases as θ increases, while for the cases of higher Reynolds number ranging from 1500-2500, JF_2 is almost constant as θ increases. This also means that the increase of the arc length of annular groove could not enhance heat transfer effectively, but lead to an increased pressure loss.

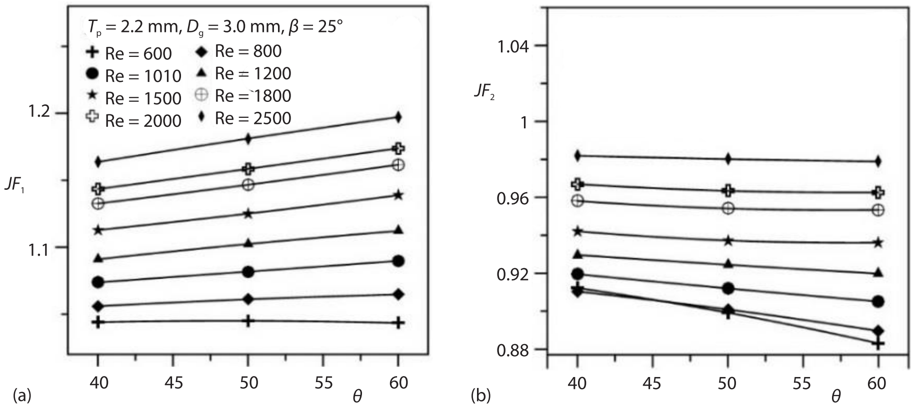

Figure 11. The relationship between thermal performance factor *JF* and arc length of the groove θ at different Reynolds number; (a) JF_1 and (b) JF_2

The correlations with including the published data

The correlations of $\mathrm{Nu_m}$ and f are very important for application of IAGF in the design process of finned tube exchanger. Too many geometric parameters are involved in IAGF, and the present study mainly focuses on three geometric parameters effects including the effects of D_g, θ, and T_p due to the limitation of computational time cost. Fortunately, Lin *et al.* [19] have obtained the fin side thermal performance of the four rows tube exchanger with IAGF. Therefore, the data presented in Lin *et al.* [19] is included to measure the correlations of $\mathrm{Nu_m}$ and f. The reason for the two sets of data could be integrated is that the tube rows have less impact on the IAGF's thermal performance. That is the periodic characteristics of thermal and flow are enough strong for multi-row tube structure, which results in the developing of the velocity and temperature boundary-layer only playing a limited role in average thermal performance.

Using a multiple non-linear regression analysis method, the correlations of $\mathrm{Nu_m}$ and f are measured with multi-parameter s including Reynolds number, D_g, D_1, T_p, θ, and β, respectively:

$$\mathrm{Nu_m} = 0.4302\mathrm{Re}^{0.5078}\left(\frac{D_g}{D}\right)^{0.1902}\left(\frac{D_1}{D}\right)^{-0.4138}\left(\frac{T_p}{D}\right)^{-0.2620}\left(\frac{\theta}{90}\right)^{0.09437}\left(\frac{\beta}{90}\right)^{-0.0176} \quad (18)$$

$$f = 16.1965\mathrm{Re}^{-0.4150}\left(\frac{D_g}{D}\right)^{0.2573}\left(\frac{D_1}{D}\right)^{0.4545}\left(\frac{T_p}{D}\right)^{-0.8636}\left(\frac{\theta}{90}\right)^{0.0891}\left(\frac{\beta}{90}\right)^{0.0289} \quad (19)$$

where $600 \le \mathrm{Re} \le 2500$, $0.14 \le T_p/D \le 0.24$, $0.22 \le D_g/D \le 0.44$, $1.15 \le D_1/D \le 1.45$, $40° \le \theta \le 60°$, and $15° \le \beta \le 30°$, and the maximum deviations of both the fitting formula and the calculation results are less than 10% for $\mathrm{Nu_m}$ and f. Moreover, one cannote from eqs. (18) and (19) that Reynolds number, the groove diameter D_g, and the arc length of the groove θ have positive effect on $\mathrm{Nu_m}$, while the other parameters including the radial location of the groove D_1, and the fin spacing T_p, and the circumferential location of the groove β have negative effect. Both θ and β have limited effect on $\mathrm{Nu_m}$. One can also note from eq. (19) that the main geometrical parameters that influence f in turn are the fin pitch T_p, the radial location of the groove D_1, and the groove diameter D_g.

To clear the mechanism of heat transfer augmentation which results from the secondary flow generated by IAGF, the secondary flow strength of all studied cases is calculated, and the relationship between Se_m and $\mathrm{N}u_m$ is obtained:

$$\mathrm{Nu_m} = 0.7503 Se_m^{\ 0.4017} \tag{20}$$

This indicates that $\mathrm{Nu_m}$ has a significant correlation with Se_m, and $\mathrm{Nu_m}$ increases with increasing Se_m.

Conclusions

To clear the parametric influences of IAGF on thermal-hydraulic characteristics for further optimizing design of this type fin pattern, a numerical simulation is conducted to discuss the influences of the geometrical parameters mainly including the annular groove diameter, the groove arc length, and the fin spacing, on the thermal performance of IAGF when Reynolds number ranges from 600-2500. For practicality, the data obtained by present study and those reported data in Lin *et al.* [19] is put together to measure the correlations of $\mathrm{Nu_m}$ and f. The findings would be quite meaningful for designing the finned circular tube heat exchanger. Given that the present study focused parametric influences on laminar convective heat transfer, it is necessary to be further stretched to turbulent convective heat transfer applications in subsequent studies. The main research conclusions are as follows.

- In contrast to PF, IAGF can significantly strengthen the fin side thermal performance. For the studied cases, the maximum heat transfer augmentation factor could reach about 1.2 under the same pumping power constraint. This should be attributed to the discontinue annular grooves which could extra induce the secondary flow.
- The parameters of the groove and working conditions have effect with different extents on the thermal performance of IAGF, and the correlations of $\mathrm{Nu_m}$ and f with Reynolds number, D_g, D_1, T_p, θ, and β are obtained. For studied cases, Reynolds number, D_g, and θ have positive effect on $\mathrm{Nu_m}$, but D_1, T_p, and β have negative effect, while the main geometrical parameters that influence f in turn are T_p, D_1, and D_g.
- Close relationship exists between the dimensionless parameter describing the mean secondary flow strength and the mean Nusselt number. But this is not the case for the fiction factor. This indicates that the studied IAGF convective heat transfer depends mainly on the secondary flow strength.
- For the studied cases in this paper, under identical pumping power constraint, the optimal D_g depends closely on Reynolds number. For the higher Reynolds number ranging from 1500-2500, the optimal D_g is about 3.5 mm, while for the lower Reynolds number ranging from 600-1500, the optimal D_g is about 3.0 mm. Under the same mass-flow rate constraint, the optimal D_g is scarcely dependent on Reynolds number, and the optimal D_g is about 2.5 mm.

Acknowledgment

This study was funded by the National Natural Science Foundation of China (51676093), the Gansu Provincial Foundation for Distinguished Young Scholars (1506RJDA061), the Transformation of S&T achievements in Universities of Gansu Province (2018D-12), and the Foundation of a Hundred Youth Talents Training Program of Lanzhou Jiaotong University.

Nomenclature

c_p – specific heat capacity, [kJkg^{-1}K^{-1}]
D – tube outer diameter, [m]
D_g – diameter of the annular groove, [m]
D_1 – diameter of the inner circular of groove, [m]
D_2 – diameter of the outer circular of groove, [m]
f – friction factor, [–]
JF – thermal performance factor, [–]
h – heat transfer coefficient, [Wm^{-2}K^{-1}]
J^n_{ABS} – absolute vorticity flux, [s^{-1}]
L_f – lengthen of the fin, [m]
N – number of tube row, [–]
Nu – Nusellt number, [
Re – Reynolds number, [–]
S_1 – horizontal spacing of circular tube, [m]
S_2 – longitudinal spacing of circular tube [m]
Se – non-dimensional parameter to describe the secondary flow strength, [–]
T – temperature, [K]
T_f – reference temperature, [K]
T_p – fin spacing, [m]
u_{in} – velocity at inlet cross-section [ms^{-1}]
x, y, z – co-ordinates axes, [m]

Greek symbols

β – circumferential position of annular groove, [°]
θ – arc length of the groove, [°]
λ – thermal conductivity, [Wm^{-1}K^{-1}]

Subscripts

f – fin
in – inlet
local – local value
m – average
out – outlet
t – tube

References

[1] Li, M. J., *et al*., Experimental and Numerical Study and Comparison of Performance for Wavy Fin and a Plain Fin with Radiantly Arranged Winglets around Each Tube in Fin-and-Tube Heat Exchangers, *Applied Thermal Engineering*, *133* (2018), Mar., pp. 298-307
[2] Moreno, R. R., *et al*., Numerical Optimization of a Heat Exchanger with Slit Fins and Vortex Generators Using Genetic Algorithms, *International Journal of Refrigeration*, *119* (2020), Nov., pp. 247-256
[3] Wang, Y., Numerical Study of Hydrodynamics and Thermal Characteristics of Heat Exchangers with Delta Winglets, *Thermal Science*, *24* (2020), 1A, pp. 325-338
[4] Okbaz, A., *et al.*, An Experimental, Computational and Flow Visualization Study on the Air-Side Thermal and Hydraulic Performance of Louvered Fin and round Tube Heat Exchangers, *International Journal of Heat and Mass Transfer*, *121* (2018), June, pp. 153-169
[5] Wang, C. C., *et al*., Investigation of the Semi-Dimple Vortex Generator Applicable to Fin-and-Tube Heat Exchangers, *Applied Thermal Engineering*, *88* (2015), Sept., pp. 192-197
[6] Wu, X. H., *et al*., Heat Transfer and Thermal Resistance Characteristics of Fin with Built – In Interrupted Delta Winglet Type, *Heat Transfer Engineering*, *37* (2016), 2, pp. 172-182
[7] Torii, K., *et al*., Heat Transfer Enhancement Accompanying Pressure-Loss Reduction with Winglet-Type Vortex Generators for Fin-Tube Heat Exchangers, *International Journal of Heat and Mass Transfer*, *45* (2002), 18, pp. 3795-3801
[8] Allison, C. B., Dally, B. B., Effect of a Delta-Winglet Vortex Pair on the Performance of a Tube – Fin Heat Exchanger, *International Journal of Heat and Mass Transfer*, *50* (2007), 25, pp. 5065-5072
[9] He, Y. L., *et al.*, Analysis of Heat Transfer and Pressure Drop for Fin-and-Tube Heat Exchangers with Rectangular Winglet-Type Vortex Generators, *Applied Thermal Engineering*, *61* (2013), 2, pp. 770-783
[10] Naik, H., Tiwari, S., Thermal Performance Analysis of Fin-Tube Heat Exchanger with Staggered Tube Arrangement in Presence of Rectangular Winglet Pairs, *International Journal of Thermal Sciences*, *161* (2021), Mar., 106723
[11] Huisseune, H., *et al*., Performance Enhancement of a Louvered Fin Heat Exchanger by Using Delta Winglet Vortex Generators, *International Journal of Heat and Mass Transfer*, *56* (2013), 1-2, pp. 475-487

[12] Leu, J. S., *et al.*, Heat Transfer and Fluid-flow Analysis in Plate-Fin and Tube Heat Exchangers with a pair of Block Shape Vortex Generators, *International Journal of Heat and Mass Transfer, 47* (2004), 19, pp. 4327-4338

[13] Gong, B., *et al.*, Heat Transfer Characteristics of a Circular Tube Bank Fin Heat Exchanger with Fins Punched Curve Rectangular Vortex Generators in the Wake Regions of the Tubes, *Applied Thermal Engineering, 75* (2015), Jan., pp. 224-238

[14] Lin, Z. M., *et al*., Numerical Study of Flow and Heat Transfer Enhancement of Circular Tube Bank Fin Heat Exchanger with Curved Delta-Winglet Vortex Generators, *Applied Thermal Engineering*, *88* (2015), Sept., pp. 198-210

[15] Lin, Z. M., *et al*., Thermal and Flow Characteristics of a Channel Formed by Aligned Round Tube Bank Fins Stamped with Curve Delta-Winglet Vortex Generators, *Thermal Science and Engineering Progress*, *26* (2021), Dec., 101113

[16] Lin, Z. M., *et al.*, Heat Transfer Augmentation Characteristics of a Fin Punched with Curve Trapezoidal Vortex Generators at the Rear of Tubes, *Thermal Science*, *26* (2022), 4B, pp. 3529-3544

[17] Oh Y., Kim K., Effects of Position and Geometry of Curved Vortex Generators on Fin-Tube Heat-Exchanger Performance Characteristics, *Applied Thermal Engineering*, *189* (2021), May, 116736

[18] Wang, C. C., *et al*., Flow Visualization of Annular and Delta Winglet Vortex Generators in Fin-and-Tube Heat Exchanger Application, *International Journal of Heat and Mass Transfer*, *45* (2002), 18, pp. 3803-3815

[19] Lin, Z. M., *et al*., Numerical Study on Heat Transfer of Circular Tube Bank Fin Heat Exchanger with Interrupted Annular Groove Fin, *Applied Thermal Engineering*, *73* (2014), 2, pp. 1465-1476

[20] Jiang, G. D., Heat Transfer and Pressure Drop of Tube Banks with Interrupted Half Annular Groove Fin (in Chinese), *Journal of Chemical Industry and Engineering*, *51* (2000), 5, pp. 604-608

[21] Zhang, Y. H., *et al*., Study of Heat Transfer Performance of Tube-Fin Heat Exchanger with Interrupted Annular Groove Fin, *Proceedings*, Int. Conference on Consumer Electronics, Communications and Networks (CECN et 2011), Xianning, China, 2011

[22] Tao, W. Q., *Numerical Heat Transfer* (in Chinese), 2nd ed., Xi'an Jiaotong University Press, Xi'an, China, 2001

[23] Wang, L. C., *et al.*, The Characteristic Temperature in the Definition of Heat Transfer Coefficient on the Fin Side Surface in Tube Bank Fin Heat Exchanger, Numerical Heat Transfer – Part A: *Applications*, *60* (2011), 10, pp. 848-866

[24] Lin, Z. M., *et al.*, The Relationship Between Absolute Vorticity Flux Along the Main Flow and Convection Heat Transfer in a Tube Inserting a Twisted Tape, *Heat and Mass Transfer*, *45* (2009), 11, pp. 1351-1363

[25] Lin, Z. M., *et al*., Characteristics of the Absolute Vorticity Flux along the Main Flow Direction on the Cross-section of the Channel Formed by Oval Tube Bank Fins, Numerical Heat Transfer – Part A: *Applications*, *57* (2010), 9, pp. 666-690

[26] Lin, Z. M., The Characteristics of Secondary Flow Heat Transfer Enhancement in Circular Tube with Twisted Tape or Vortex Generators (in Chinese), Ph. D. thesis, Lanzhou Jiaotong University, Jiaotong, China, 2011

[27] Eiseman, P. R., A Multi-Surface Method of Co-ordinate Generation, *Academic Press*, *33* (1979), 1, pp. 118-150

[28] Eriksson, L. E., Practical Three-Dimension Mesh Generation Using Transfinite Interpolation, *Siam J. Sci. Stat. Comp*., *6* (1985), 3, pp. 712-741

[29] Li, Z. Y., Tao, W. Q., A New Stability-Guaranteed Second-Order Difference Scheme, Numerical Heat Transfer – Part B: *Fundamentals*, *42* (2002), 4, pp. 349-365

[30] Rhie, C. M., Chow, W. L., Numerical Study of the Turbulent Flow Past an Airfoil with Trailing Edge Separation, *AIAA J*, *21* (1983), 11, pp. 1525-1532

[31] Yun, J. Y., Lee, K. S., Influence of Design Parameters on the Heat Transfer and Flow friction Characteristics of the Heat Exchanger with Slit Fins, *Int. J. Heat Mass Transfer*, *43* (2000), 14, pp. 2529-2539

Paper submitted: October 15, 2021
Paper revised: November 5, 2021
Paper accepted: November 24, 2021